Crack Front Geometry and Stress Intensity Factor of Semi-Circular Bend Specimens with Straight Through and Chevron Notches

Yuzo Obara[a]*, Kimiharu Nakamura[b], Singo Yoshioka[c], Atsushi Sainoki[a], Akira Kasai[a]

[a]*Kumamoto University, Kumamoto, Japan*
[b]*JST Co. Ltd., Kita-kyushu, Japan*
[c]*Shimizu Corporation, Tokyo, Japan*
* *obara@kumamoto-u.ac.jp*

Abstract

The semi-circular bending (SCB) test is one of the most useful testing methods for determining the mode-I fracture toughness of rocks. A SCB specimen with an artificial notch is loaded at three points including two lower points and a single upper point during the test. In general, there are two types of geometries for artificial notches: straight through and chevron notches. The straight through notch is commonly adopted for the SCB (STNSCB) test as the suggested method for estimating mode-I fracture toughness of rocks in ISRM, while the cracked chevron notch SCB (CCNSCB) test using a specimen with a chevron notch has been performed by some researches. In this paper, by means of the commercial finite element software ABAQUS, cracking behavior from the tip of an artificial notch during STNSCB and CCNSCB tests is analyzed with Extended Finite Element Method (XFEM) in order to clarify crack front geometry in the process of cracking. The relationship between the crack length and the stress intensity factor can be obtained by analyzing stress intensity factors of the specimen with FEM, based on crack front geometries calculated with XFEM during the cracking process. Using this relationship, the minimum stress intensity factor at a critical crack length is determined for estimating mode-I fracture toughness of the rock for the CCNSCB test. Furthermore, by performing the SCB tests using Kimachi sandstone specimens with three different artificial notch geometries, fracture toughness of the sandstone is determined from the SCB test. Consequently, it is concluded that the values of fracture toughness from the test with three notch geometries are almost the same.

Keywords: SCB test, Chevron notch, Geometry of crack front, Stress intensity factor, FEM, Fracture toughness

1. Introduction

Extremely long-term stability of rock mass is occasionally required for various engineering projects, including high-level nuclear waste disposals and caprocks for carbon capture storage. For this purpose, it is important to consider the strength of the bedrock around these rock mass structures. For the design of such rock mass structures, uniaxial compressive and tensile strengths are used as a rock strength parameters. These are deemed to be macroscopic mechanical properties. It can become necessary to understand the fracturing behavior of rock mass for the design and stability evaluation, especially in such a case that extremely long-term stability needs to be achieved considering fracture initiation and propagation. In the fracturing process of rock, fracture toughness, which is a microscopic mechanical property and represents critical resistance to the crack propagation, should be considered.

In order to measure the fracture toughness of rock, several methods have been proposed by the International Society for Rock Mechanics (ISRM): Chevron bend (CB) test and Short Rod (SR) test by Ouchterlony (1988); Cracked Chevron Notched Brazilian Disc (CCNBD) test by Fowell (1995); Semi-circular Bend (SCB) test by Kuruppu, Obara *et al.* (2014) etc. The SCB testing method, which was proposed originally by Chong and Kuruppu (1984), has recently received much attention from researchers. The specimen used for the SCB test is a semi-circular disk with either a straight notch (Straight Through Notch SCB: STNSCB) or chevron notch (Cracked Chevron Notched SCB: CCNSCB). These experimental configurations are shown in Fig.1.

The SCB test is convenient, because of its straightforward way to prepare the specimen, thus having been added to the ISRM suggested methods. Its compact shape, formed by cutting a core into slices and duplicating half semi-circular disks, is suitable for conveniently investigating the effects of various parameters such as strain rate, moisture content, and temperature (Karfakis 1986, Funatsu et al. 2004) as well as loading rate, size, and confining pressure (Kataoka et al. 2014a, 2015, 2017) on the fracture toughness of rocks. Using this specimen type, the anisotropy of the fracture toughness (Kataoka et al. 2014b), and mode-II or mixed mode fracture toughness can also be investigated (Chong et al. 1987, 1988; Lim et al. 1993, 1994a, 1994b). The SCB test was also used for evaluating the dynamic fracture toughness (Zhou et al. 2012, Du et al. 2017). Thus the STNSCB test is used to determine fracture toughness of rock.

On the other hand, several studies concerning the SCB test were recently undertaken resulting in the creation of the CCNSCB specimen with a curved chevron notch. When a chevron notch is used, a sharp natural crack is created in the specimen and the crack resistance of the material should became fully developed with the initial crack growth (Ouchterlony 1988). However, Wei et al. (2016a, 2016b) assumed that the crack initiates from the crack tip and propagates via a straight crack front along the notched plane. Stress intensity factors at any stage during the fracture propagation were determined by means of a finite element analysis. At the same time, the SCB tests using the STNSCB and the CCNSCB specimens of sandstone and granite were performed to compare the results derived from specimens with

different notch shapes (Wei at al. 2016b). It was noted that the CCNSCB method is reliable for determining the fracture toughness of rocks in their work. Wei et al. (2017a) examined the fracture toughness of rock for the CCNBD and the CCNSCB specimens, considering the fracture process zone. Then, the fracture toughness obtained from each test was compared. Wei et al. (2017b) analyzed stress intensity factors of the STNSCB and the CCNSCB specimens, considering the fracture process zone. In this analysis, it was postulated that the crack geometry is a curved chevron notch, and its crack front geometry during propagation was assumed to be straight. Subsequently, a comparison was made in terms of the fracture toughness calculated based on the assumption. It was noted by the author that the CCNSCB method is less influenced by the presence of the fracture process zone than the STNSCB method. Mahdavi et al. (2015) investigated the stress intensity factor for CCNSCB specimens with a straight chevron notch using the finite element method. They pointed out that the high stress concentration is produced at the two corners of the crack front propagating via a straight front along the notched plane. In light of the result, they modified the shape of rounded corners in the analysis. The result was compared to that with a slice synthesis method (SSM). Ayatollahi et al. (2016) analyzed the stress intensity factor of the STNSCB and the CCNSCB specimens. The CCNSCB specimen has a curved chevron notch, and its front geometry of during the propagation has rounded corners. Aliha et al. (2017) performed the analysis of stress intensity factor and T-stress of three types of specimens, including the CCNSCB specimen with a curved chevron notch and a straight crack front.

The chevron notch may have an advantage over the straight notch. By concentrating stress on the chevron notch tip, the crack initiates from the tip at a relatively low load. The crack propagation during loading is considered to occur under natural conditions rather than artificially produced. However, it is still quite challenging to determine the crack front geometry during crack propagation. Dai et al. (2015) investigated the progressive failure during the fracture toughness test suggested by ISRM using the Rock Failure Process Analysis (RFPA) software. The CB and SR specimens with a chevron notch were analyzed, showing that the crack front geometry is an arc, which is deemed more realistic. They indicated that the actual critical crack length is significantly different from that of an ideal situation. The stress intensity factor of the CCNSCB specimen has been analyzed under the ideal situation, in which the crack propagates via a straight crack front along the notched plane. Therefore, it is necessary that the stress intensity factor of the CCNSCB specimen is analyzed with a more realistic crack front geometry during crack propagation. That is, the cracking behavior of the chevron notch during crack initiation/propagation should be analyzed to clarify and identify the geometry of the crack front. Then, the stress intensity factor ought to be calculated from the obtained geometry of the crack front, whereby the minimum normalized stress intensity factor can be determined to estimate the mode-I fracture toughness. This allows us to compare the fracture toughness estimated from the CCNSCB to that of the STNSCB test. It is of great interest to investigate whether those values are comparable because several studies suggest using fracture toughness estimated from STNSCB tests based on the method by Kuruppu, Obara et al. (2014). If comparable, the STNSCB test is more convenient for determining the

fracture toughness of rock because of its simplicity of sample preparation. For the purpose of clarifying this problem, a detailed investigation of the cracking behavior of both cases with different crack geometries is indispensable.

There is another problem in analyzing the stress intensity factor of the CCNSCB specimen. In order to calculate the normalized stress intensity factor of the CCNSCB, previous studies basically employed numerical methods such as the finite element method. For instance, static analyses were performed by Ayatollahi et.al (2016) using numerical models that simulate crack propagation with a straight crack front, as shown in Fig.2. As for the modelling method, they indicated a problem that the stress distribution was not uniform along the straight crack front in Fig.2(b), and high stress concentrations were induced at both corners of the crack front. The crack can propagate at both the corners due to the stress concentration. A modified model was then prepared to overcome the issue, so that the stress distribution becomes uniform along the crack front while decreasing these high stress concentrations as shown in Fig.2(c). Subsequently, a reasonable crack front geometry was determined through trial and error in this case. As described above, it is not straightforward to delineate the crack front geometry. Therefore, it is of paramount importance that geometrical change in the crack front during crack propagation is examined with a numerical method, and the stress distribution along the crack front is analyzed using the determined crack front geometry during the propagation.

In this study, the cracking behavior of the notch is first analyzed for the STNSCB and CCNSCB tests through the ABAQUS software, employing an extend finite element method (XFEM) to clarify the crack front geometry in the process of cracking. Next, using FEM, the stress intensity factor is computed for the 3D models with different crack front geometries on various loading stages during the XFEM analyses. Then, the relation between the crack length and the stress intensity factor is obtained precisely. From these analyses, the critical crack front geometry at the maximum load as well as the minimum normalized stress intensity factor is determined for estimating the mode-I fracture toughness of rock specimens for the STNSCB and CCNSCB test. Furthermore, performing the STNSCB and CCNSCB tests using specimens of Kimachi sandstone, the values of fracture toughness are separately determined for specimens with three different artificial notch geometries using the obtained minimum stress intensity factor by the analysis. Based on the experimental results, it was concluded that the STNSCB test is more convenient than the CCNSCB test in terms of the estimation of fracture toughness because that i) both the test methods produce comparable fracture toughness and ii) the specimen for the STNSCB test can be readily prepared, compared to that for the CCNSCB test.

2. STNSCB and CCNSCB test

A STNSCB specimen is delineated in Fig.1(a). Its fracture toughness is estimated with the following equation (Kuruppu et al. 2014):

$$K_{\mathrm{IC}} = \frac{P_{\max}\sqrt{\pi a}}{2Rt} Y_{\mathrm{I}} \tag{1}$$

where Y_I is a normalized stress intensity factor at the maximum load.

On the other hand, geometrical configuration and corresponding parameters for the CCNSCB test are illustrated in Fig.1(b). The specimen has a chevron notch with a chevron angle of θ and is loaded at three points including the lower two points and the upper single point. Mode-I fracture toughness K_{IC} of the CCNSCB specimen can be determined with the following equation (Fowell 1995):

$$K_{IC} = \frac{P_{max}}{t\sqrt{R}} Y^* \tag{2}$$

where R and t are radius and thickness of the specimen, respectively; P_{max} is the maximum load; and Y^* is the normalized stress intensity factor at the maximum load. The Y^* can be obtained as the minimum value during the crack propagation. This equation was suggested for the CCNBD test. In this study, the same type equation was adopted.

In the case of the CCNSCB test, the primary crack initiates from the tip of the artificial chevron notch and then grows upward, refer to Fig.1(b) for the geometry. However, the crack propagation from the chevron notch and the critical crack front geometry at the maximum load have not yet been accurately determined. Therefore, the process of the crack propagation and the stress intensity factor along the crack front are examined and numerically analyzed in the following chapters.

3. Numerical simulation of STNSCB and CCNSCB test with XFEM

3.1 Outline of XFEM

An extend finite element method (XFEM) analysis is employed to investigate how the crack front geometry varies during crack propagation. Then, a FEM analysis is performed for calculating stress intensity factor based on the geometry of the crack front obtained from the XFEM analysis. To determine crack front geometries during crack propagation regarding the STNSCB and CCNSCB tests, an XFEM analysis is performed with three-dimensional finite element software ABAQUS. The extended finite element method was first introduced by Belytschko and Black (1999). It is an extension of the conventional finite element method based on the concept of partition of unity proposed by Melenk and Babuska (1996), which allows local enrichment functions to be easily incorporated into a finite element approximation. The presence of discontinuities is ensured by the special enriched functions in conjunction with additional degrees of freedom. Crack initiation and propagation can be analyzed with ABAQUS as a quasi-static problem. In the case of FEM analysis, modeling a growing crack is cumbersome because the mesh must be updated continuously to match the geometry of the discontinuity as the crack progresses, whereas in the case of XFEM, it is possible to investigate crack propagation without re-meshing the crack front in the XFEM analysis. The details of the enrichment functions and the other features introduced in ABAQUS are described in the user's manual (2018). The important theories to simulate crack propagation with XFEM will be summarized in the following section.

3.2 Cohesive behavior of crack element

A crack propagation analysis uses cohesive elements with traction-separation constitutive behavior as the enriched element as follows: The available traction-separation model assumes initially linear elastic behavior followed by the initiation and evolution of damage. The elastic behavior is described in terms of an elastic constitutive matrix that relates the normal and shear stresses to the normal and shear separations of a cracked element.

The nominal traction stress vector $\{t\}$, consists of the following components: t_n, t_s, and t_t, which represent the normal and the two shear tractions, respectively. The corresponding separations are denoted by δ_n, δ_s and δ_t. The elastic behavior can then be written as

$$\{t\} = \begin{Bmatrix} t_n \\ t_s \\ t_t \end{Bmatrix} = \begin{bmatrix} K_{nn} & 0 & 0 \\ 0 & K_{ss} & 0 \\ 0 & 0 & K_{tt} \end{bmatrix} \begin{Bmatrix} \delta_n \\ \delta_s \\ \delta_t \end{Bmatrix} = [K]\{\delta\}$$

where the terms K_{nn}, K_{ss} and K_{tt} are calculated based on the elastic properties for an enriched element.

When the maximum principal stress reaches the specified crack initiation stress σ_{cri}, the crack initiates and the newly introduced crack is always orthogonal to the maximum principal stress orientation. Then, the crack propagates as the linear traction-separation response with a failure mechanism shown as the damage model in Fig. 3. In the figure, the normal cohesive traction decreases with the increasing crack opening and becomes zero at δ_{max}. The crack surface is completely separated at that time.

3.3 Model of specimen

Three types of 3D extend finite element models representing the SCB specimens are depicted in Fig.4. The upper one is the numerical model for a STNSCB specimen with a straight notch, and the middle and lower ones are the models of the CNNSCB specimens with different chevron notches with angles of 90 and 75 degrees, respectively. The mechanical properties of the elastic medium are set as E=2.9GPa and v=0.23, which were experimentally obtained from sandstone specimens. Then, the parameters σ_{cri} and δ_{max} are assumed to be 15 MPa and 0.02 mm, respectively. The validity of the input parameters is investigated and confirmed in a later section. Geometric and mechanical parameters of the specimen are summarized in Table 1. The number of nodes and elements used for the numerical models are listed in Table 2.

3.4 Load-displacement curve and crack propagation

First, in order to confirm the validity of the parameters used for the analysis, the load-displacement curve obtained from STNSCB test with sandstone was compared to that derived from the XFEM analysis using the STNSCB model as shown in Fig.5. The experimental curve is characterized as a downward convex at the low load level and changes to a linear curve thereafter until the maximum load. Compared to the experimentally-derived curve, the analyzed curve appears linear until the maximum load. Although the behavior at the low load level and maximum load are slightly different between the results, it is reasonable to conceive that these results are almost identical. The analysis did not converge when the load decreases after passing the maximum load, meaning that unstable crack propagation is initiated. Importantly, the same behavior was observed in the experiment. Thus, both the results indicate

that the numerical analysis result is consistent with the experimental result. Therefore, it is concluded that the parameters used are reasonable and can be applied to the following analyses.

The analyzed states of crack propagation correspond to the numerical numbers depicted on the curve in Fig.5, and analysis results at those states are shown in Fig.6. The state of crack opening is represented by STATUSXFEM parameter, which indicates the status of the element with a value between 0 and 1.0. A value of 1.0 denotes "completely fractured or separated" and δ_{max} equals to 0.02 mm. The red color represents the area where the crack opening displacement is more than 0.02 mm. In state 1 (589N), the crack initiated from the chevron tip and slightly propagated except at the ends of the crack. In state 2 (764N), i.e. at the maximum load, the propagation progressed, and the crack front is about 1.2 mm from the chevron tip.

Based on these analyses, the cross-sectional geometry of the crack front for each crack length can be determined as shown in Fig.7. As can be seen from the figure, the central part of the crack front progresses forward more, yielding the concave curves. The distance from the bottom of the specimen to the crack front on the centerline is assumed to be the crack length a. The relations between load and normalized crack length a/R of the STNSCB model derived from the XFEM analysis are shown in Fig.8. The curve is characterized as a convex approaching the maximum load. The analysis was stopped when the applied load passed the maximum load and the crack length of a/R reached 0.54, because the numerical analysis became unstable.

Next, the load-displacement curve and crack propagation states obtained from CCNSCB test simulations with chevron angles of 90 and 75 degrees are shown in Fig.9 and Fig.10, respectively. The crack initiation occurs from the chevron tip, and it is confirmed that crack propagates upward at around the maximum load. It is noted from this analysis that the zero boundary of the STATUSXFEM parameter is not smooth because this depends on the finite element mesh arrangement. Nevertheless, the crack front geometry can be determined during the loading of the CCNSCB test whilst tracing the boundary smoothly.

The relations between the load and the normalized crack length a/R of the CCNSCB models for the XFEM analysis are shown in Fig.11. The crack length a is assumed to be the distance from the bottom of the specimen to the crack front on the centerline. The curve is characterized as a concave curve and approaches the maximum load. The analysis was stopped when the applied load passed the maximum load because computational instability occurred due to abrupt and unstable crack propagation. At that time, the ratio a/R reached 0.39 for the model having a chevron notch with 90 degrees and 0.38 for the model with 75 degrees. Importantly, these crack lengths are considered close to the critical crack length.

4. Determination of stress intensity factor with FEM

4.1 3D model

The change in the crack front geometry during the STNSCB and CCNSCB tests was determined in the previous section. The stress intensity factor is then analyzed with FEM, using 3D models with different crack front geometries at different loading stages during the XFEM analysis. The distribution of stress intensity factor along the crack front is calculated with the *J*-integral method. The mechanical properties and model dimensions are the same as those of the XFEM analysis.

An example of the 3D FEM model is shown in Fig.12. This was constructed based on the geometry of the crack front obtained from the XFEM analysis. It is also important to consider the occurrence of singularities when modelling the crack. To precisely represent the stress concentration at the crack tip, the crack front was discretized with wedge elements, and hexahedral elements are assigned to the rest of the contour integral region.

4.2 Normalized stress intensity factor

To obtain the minimum normalized stress intensity factor during the crack propagation, four and eight different models are prepared for the STNSCB and the CCNSCB specimens, respectively. The crack length ratio a/R ranges from 0.5 to 0.54 for the STNSCB specimens and from 0.3 to 0.55 for the CCNSCB specimens.

The distribution of the normalized stress intensity factor from the STNSCB is analyzed for each model with the crack front geometry obtained from the XFEM analysis, as shown in Fig.13. The magnitude is smaller at both the corners and distributed on an arc, while in the middle part of the crack front the distribution is found to be almost uniform. Therefore, the average value of the normalized stress intensity factors along the crack front is calculated to be in the range of 5 to 25 mm in the *x*-coordinate. Fig.14 shows the relationship between the average normalized stress intensity factor and normalized crack length. The stress intensity factor increases linearly with increasing crack length. The minimum value of the normalized stress intensity factor occurs at an a/R of 0.5, which corresponds to the value before the crack propagates, i.e. the original straight notch. The minimum value is 6.67, which approximates 6.65 shown in the ISRM suggested method. Therefore, the XFEM and FEM analyses demonstrated that the fracture toughness of STNSCB test can be estimated using the original formulation of ISRM.

In the case of the CNNSCB with a chevron angle of 90 degrees, the analysis was stopped when the applied load reached the maximum value at an a/R of 0.39 because computational instability occurs. Since it is quite challenging to analyze the crack propagation at post-peak load, the crack front geometries after the maximum load are assumed to be similar to that around the middle part of crack front at an a/R of 0.39. Fig.15 depicts the cross-sectional geometry of the crack front for each crack length. Using numerical models with these crack fronts, the FEM analysis was performed to calculate stress intensity factors along the crack front. The distribution of the stress intensity factors in the range of 0.3 to 0.55 is shown in Fig.16.

In the initial state ($a/R = a_0/R$=0.30), the normalized stress intensity factor shows a high value locally at the central part. Therefore, high stress concentration is induced at the tip of the artificial chevron notch, and it is straightforward to imagine that the crack may initiate from that part. The normalized stress intensity factor at the crack tip becomes smaller and more uniform as the crack propagates. Then, its distribution changes from a higher concentration at the center to a more uniform shape with the increasing load. In this study, the average value of the uniform section at middle part of the crack with a width of 11mm is defined as the normalized stress intensity factor.

The relationship of the normalized stress intensity factor with respect to a/R is shown in Fig.17. This result demonstrates that the normalized stress intensity factor first decreases and then increases with an increasing a/R ratio. In this case, the normalized stress intensity factor can be approximated as the following equation:

$$Y^*_{90} = 17.4 - 55.6\left(\frac{a}{R}\right) + 63.6\left(\frac{a}{R}\right)^2 \qquad (3)$$

Since the 11mm width with approximately uniform stress intensity factors corresponds to an a/R of 0.38, the normalized stress intensity factors at a/R of less than 0.38 were not used for the approximation. The approximately uniform section of the stress intensity factors along the crack front occurs during stable crack propagation after its initiation and before the transition to unstable propagation. Therefore, it is reasonable to calculate the average value based on stress intensity factors on the approximately uniform section. Using equation (3), it is concluded that the minimum stress intensity factor is 5.26 at an a/R of 0.438 in the case of the geometric parameters of the CCNSCB specimen in this paper. It is also found that the critical crack front geometry at the maximum load is similar to that when a/R is 0.43 in Fig.15.

Finally, in the case of the CCNSCB with a chevron angle of 75 degrees, a similar procedure was taken to obtain the minimum stress intensity factor. Since it is quite difficult to analyze the post-peak crack propagation, the crack front geometries after the maximum load are assumed to be similar to that around the middle part of the crack front at an a/R of 0.38. Fig.18 shows the cross-sectional geometry of the crack front for each crack length. Using numerical models with these crack fronts, the FEM analysis was performed to calculate stress intensity factors along the crack front. The distribution of the stress intensity factors in the range from 0.3 to 0.55 is shown in Fig.19.

Fig.19 shows that in the initial state ($a/R = a_0/R$=0.30), the normalized stress intensity factor shows a high value locally at the central part. The normalized stress intensity factor at the crack tip changes to be small and uniform with the crack propagation in the same way as the model with a chevron angle of 90 degrees. The stress intensity factor distribution changes from a higher concentration at the center to an approximately uniform shape with the increasing load. In this case, the normalized stress intensity factors are averaged along the approximately uniform section, which varies for each a/R in the range of thickness from 10 mm to 20 mm in the middle part of the crack front the distribution. The calculated average value is defined as normalized stress intensity factor for the crack.

The relation of the normalized stress intensity factor with respect to a/R is shown in Fig.20. This result demonstrates that the normalized stress intensity factor first decreases then increases with an increasing a/R ratio. In this case, the normalized stress intensity factor can be approximated as the following equation:

$$Y^*_{75} = 18.7 - 57.0\left(\frac{a}{R}\right) + 67.0\left(\frac{a}{R}\right)^2 \quad (4)$$

The values at less than 0.38 were not used in the approximation for the same reason as the model with a chevron angle of 90 degrees. Using equation (4), it is concluded that the minimum stress intensity factor is 6.58 at an a/R of 0.425 for the CCNSCB specimen modelled in this paper. When the normalized stress intensity factor takes the minimum value, the critical crack front geometry at that time is similar to the crack front geometry at an a/R of 0.43 in Fig.18.

5. SCB test

The geometry of the SCB specimen is the same as that shown in Fig.1. As described, loads are applied at the two points on the bottom as well as the single point on the top. Its compact geometry formed by cutting a core into slices and duplicating semi-circular disks is suitable for conveniently investigating the effect of various parameters such as loading rate, moisture content, and temperature on the fracture toughness of rocks. K_I is estimated using the equation (1) and (2). In the test, the following geometric parameters were set: s/R = 0.8 and a/R = 0.5 for the STNSCB specimen and a/R = 0.3 for the CCNSCB specimen. These conditions are the same as the analysis.

The Kimachi sandstone used for this testing work is tuffaceous sandstone. The grains are mainly composed of andesite clastics with average diameters of 0.4–0.6 mm (Kataoka et al. 2013). The porosity of this rock is approximately 20 % (Takahashi et al. 2011). Other material properties of Kimachi sandstone are summarized in Table 3 (Kataoka *et al.* 2019).

Examples of fractured surfaces of STNSCB and CCNSCB specimens after the test are shown in Fig.21. As can be seen, the straight and chevron notches are pre-formed geometry.

To investigate crack initiation, the SCB tests were performed for STNSCB and CNNSCB specimens with a chevron angle of 90 degrees whilst monitoring acoustic emission (AE). An AE sensor was attached to the side surface of the specimen as shown in Fig.22. The AE signals were amplified by 40 dB and recorded using a computer with appropriate software (AEwin, Physical Acoustics Corporation). A threshold of 45 dB was selected and a band-pass filter with a range of 100 kHz to 2 MHz was used. The load and cumulative AE event during the test are shown in Fig.23. The load-displacement curve is normalized using the maximum load P_{max} and the displacement at P_{max}, respectively. The load-displacement curve forms a downward convex at a low load level and changes to a linear curve thereafter until the specimen is fractured at the maximum load in both the tests. In the STNSCB test, the AE events are rarely recorded until the load reaches 97 % of P_{max} and then the cumulative AE event drastically rises immediately after the load reaches P_{max}. This result demonstrates that the crack initiates

near P_{max} and propagates rapidly just after the initiation, entailing microcracking. This agrees well with those derived from the STNSCB test of Rustenburg granodiorite performed by Kataoka (2014). On the other hand, in the CCNSCB test, the load-displacement curve is almost the same as the STNSCB test. However, the AE activity starts at 93% of P_{max} and increases linearly, and then the cumulative AE event rises rapidly until the load reaches P_{max}. This result indicates that the crack initiates at slightly low stress level at the tip of the chevron notch, compared to the STNSCB test, and the crack propagates gradually, followed by intense fracturing around P_{max}. This behavior coincides with the results obtained from the XFEM and FEM analyses.

Finally, the load-displacements curves for all the specimens are summarized in Fig. 24. The fracture toughness of Kimachi sandstone was estimated from the specimens with different artificial notch geometries as shown in Fig. 25. The results are listed in Table 4, 5 and 6. In the STNCCB test, Y_I was calculated by the original formulation of ISRM. Therefore, the values of Y_I are different depending on the size of the specimen. The maximum value of the CCNSCB tests with a chevron angle of 90 degrees and the minimum value of the STNSCB tests are shown as the dotted lines in the figure. The fracture toughness values obtained from the two types of specimens are found to be distributed between the two dotted lines. On the other hand, the values of the CCNSCB specimens with a chevron angle of 75 degrees are found to be slightly higher than those of the STNSCB specimens. However, its minimum value is located at the minimum value dotted line. Allowing for variance of the measured values, it would be reasonable to consider that the values obtained from the specimens with three types of artificial notch geometries are equivalent. Hence, it can be concluded that the STNSCB test is more convenient than the CCNSCB test when estimating the fracture toughness of rock using the SCB test. Both test methods produce equivalent results and the specimen preparation for STNSCB test is more straightforward.

5. Conclusions

In order to simulate the process of crack initiation/propagation during the STNSCB and the CCNSCB tests, the XFEM analysis was first performed and the cracking behavior and crack front geometries identified for different load levels. Then, FEM analyses were conducted using models with various crack front geometries obtained from the XFEM analysis results, whereby the critical crack length as well as the minimum normalized stress intensity factor of the STNSCB and the CCNSCB specimens were determined using the critical crack front geometry.

Furthermore, by conducting the STNSCB and CCNSCB tests using specimens of Kimachi sandstone, the values of fracture toughness were determined for three different artificial notch geometries by using the obtained minimum stress intensity factor from the analysis. Finally, through comparison of the calculated fracture toughness for specimens with different notch geometries, it was concluded that the STNSCB test is more convenient than the CCNSCB test for the estimation of fracture toughness

because i) both the test methods produce equivalent fracture toughness; and ii) the specimen for the STNSCB test can be readily prepared, compared to that for the CCNSCB test.

References

Ayatollahi, M. R., Mahdavi, E, Alborzi, M. J., Obara,Y, (2016), "Stress Intensity Factors of Semi-Circular Bend Specimens with Straight-Through and Chevron Notches", Rock Mech Rock Eng 49:1161–1172, DOI 10.1007/s00603-015-0830-y.

Belytschko, T., and T. Black, (1999), "Elastic Crack Growth in Finite Elements with Minimal Remeshing", International Journal for Numerical Methods in Engineering, vol. 45, pp. 601–620.

Chong K. P, Kuruppu MD, (1984), "New specimen for fracture toughness determination of rock and other materials". Int J Fract 26: R59–R62.

Chong, K. P., Kuruppu, M. D., Kuszmaul, J. S. (1987), "Fracture toughness determination of layered materials", Eng. Fract. Mech., 28 (1), 43-54.

Chong, K. P., Kuruppu, M. D. (1988), New specimens for mixed mode fracture investigations of geomaterials, Eng. Fract. Mech., 30 (5), 701-712.

Dai, F., Wei, M.-D., Xu, N.W., Zhao, T., Xu, Y. (2015), "Numerical investigation of the progressive fracture mechanisms of four ISRM-suggested specimens for determining the mode I fracture toughness of rocks", Computers and Geotechnics 69, 424–441.

Du, H., Dai, F., Xia, K., Xu, N. Xu, Y. (2017), "Numerical investigation on the dynamic progressive fracture mechanism of cracked chevron notched semi-circular bend specimens in split Hopkinson pressure bar tests", Eng Frac Mech, 184, 202–217, doi.org/10.1016/j.engfracmech.2017.09.001.

Fowell R. J, (1995), "ISRM commission on testing methods. Suggested method for determining mode I fracture toughness using cracked chevron notched. Brazilian disc (CCNBD) specimens". Int J Rock Mech Min Sci Geomech Abstr, 32(1):57–64.

Funatsu, T., Seto, M., Shimada, H., Matsui, K. and Kuruppu, M. (2004), "Combined effects of increasing temperature and confining pressure on the fracture toughness of clay bearing rocks", Int. J. Rock Mech. Min. Sci., 41, 927-938.

https://www.sharcnet.ca/Software/Abaqus610/Documentation/docs/v6.10/books/usb/default.htm?startat=pt04ch10s06at33.html, 2018.

Karfakis MG, Chong KP, Kuruppu MD (1986), Critical review of fracture toughness testing of rocks. The 27th US Symposium on Rock.

Mechanics (USRMS) American Rock Mechanics Association.

Kataoka, M. and Obara, Y. (2013), "Estimation of fracture toughness of different kinds of rocks under water vapor pressure by SCB test", J. MMIJ, 129, 425-432 (in Japanese).

Kataoka, M., Kang, H-M., Cho, S-H., Obara, Y. (2014a), “Influence of Loading Rate on Fracture Toughness of Rock by Semi-Circular Bend (SCB) Test”, Proceedings of 8th Asian Rock Mechanics Symposium, Sapporo, Japan, PR-3-5.

Kataoka, M., Obara, Y., Kuruppu, M. (2014b), “Estimation of Fracture Toughness of Anisotropic Rocks by Semi-Circular Bend (SCB) Tests Under Water Vapor Pressure”, Rock Mech Rock Eng, 48, 4, 1353-1367, DOI 10.1007/s00603-014-0665-y.

Kataoka, M., Obara, Y. (2015), “Size Effect in Fracture Toughness of Sandstone”, Proc. of ISRM 13th International Congress on Rock Mechanics, Paper 140, ISBN: 978-1-926872-25-4.

Kataoka, M., Mahdavi, E., Funatsu, T., Takehara, T., Obara, Y., Fukui, K., Hashiba, K. (2017), ” Estimation of Mode I Fracture Toughness of Rock by Semi-Circular Bend Test under Confining Pressure Condition”, Procedia Engineering 19, 1886 – 893, doi: 10.1016/j.proeng.2017.05.258.

Kataoka M, Obara Y, Vavro L, Soucek K, Cho S-H, Jeong S-S (2019), Effect of Testing Method Type and Specimen Size on Mode I Fracture Toughness of Kimachi Sandstone. J MMIJ 135(3):33–41. https://doi.org/10.2473/journalofmmij.135.33

Lim, I. L., Johnston, I. W., Choi, S. K., 1993, Stress intensity factors for semi-circular specimens under three-point bending, Engng. Fract. Mech., 44, 363-382.

Lim, I. L., Johnston, I. W., Choi, S. K., Boland, J. N., 1994a, Fracture testing of a soft rock with semi-circular specimens under three-point bending, part 1-mode I, Int. J. Rock Mech. Min. Sci. Geomech. Abstr, 31 (3), 185-197.

Lim, I. L., Johnston, I. W., Choi, S. K., Boland, J. N., 1994b, Fracture testing of a soft rock with semi-circular specimens under three-point bending, part 2-mixed-mode, Int. J. Rock Mech. Min. Sci. Geomech. Abstr., 31 (3), 199-212.

Kuruppu MD, Obara Y, Ayatollahi MR, Chong KP, Funatsu T, (2014), “ISRM-suggested method for determining the mode I static fracture toughness using semicircular bend specimen”. Rock Mech Rock Eng, 47(1):267–74.

Mahdavia, E., Obara, Y., Ayatollahia, M. R. (2015), “Numerical investigation of stress intensity factor for semi-circular bend specimen with chevron notch”, Engineering Solid Mechanics 3, 235-244.

Melenk, J., and I. Babuska, (1996), “The Partition of Unity Finite Element Method: Basic Theory and Applications”, Computer Methods in Applied Mechanics and Engineering, vol. 39, pp. 289–314.

Ouchterlony F, (1988), “ISRM commission on testing methods. Suggested methods for determining fracture toughness of rock”. Int J Rock Mech Min Sci Geomech Abst, 25:71–96.

Reza, M., Aliha, M., Mahdavi, E., Ayatollahia, M. R. (2017), “The Influence of Specimen Type on Tensile Fracture Toughness of Rock Materials”, Pure Appl. Geophys. 174, 1237–1253, DOI 10.1007/s00024-016-1458-x.

Takahashi, M., Fuji, Y., Ahn, C., Takemura, T., Takahashi, N. and Park, H. (2011), "Microstructure in Kimachi sandstone obtained with mercury intrusion porosimetry and micro focus X ray CT structure analysis", J. Japan Society Eng. Geology, 52, 184-191 (in Japanese).

Wei, M.-D., Dai., F., Xu, N.-W., Zhao, T. (2016a), "Stress intensity factors and fracture process zones of ISRM-suggested chevron notched specimens for mode I fracture toughness testing of rocks", Engineering Fracture Mechanics 168, 174–189.

Wei, M.-D., Dai, F., Xu, N.-W., Liu, J.-F., Xu, Y. (2016b), "Experimental and Numerical Study on the Cracked Chevron Notched Semi-Circular Bend Method for Characterizing the Mode I Fracture Toughness of Rocks", Rock Mech Rock Eng 49:1595–1609, DOI 10.1007/s00603-015-0855-2.

Wei, M.-D., Dai, F., Liu, Y., Xu, N.-W., Zhao, T. (2017a), "An experimental and theoretical comparison of CCNBD and CCNSCB specimens for determining mode I fracture toughness of rocks", Fatigue Fract Eng Mater Struct, 1–17. DOI: 10.1111/ffe.12747.

Wei, M.-D., Dai, F., Xu, N.-W., Zhao, T., Liu, Y. (2017b), "An experimental and theoretical assessment of semi-circular bend specimens with chevron and straight-through notches for mode I fracture toughness testing of rocks", International Journal of Rock Mechanics and Mining Sciences 99, 28–38.

Zhou, Y. X., Xia, K., Li, X. B., Li, H. B., Ma, G. W., Zhao, J., Zhou, Z. L., Dai, F. (2012), "Suggested methods for determining the dynamiSTNrength parameters and mode-I fracture toughness of rock materials", Int. J. Rock Mech. & Min. Sci., 49, 105-112.

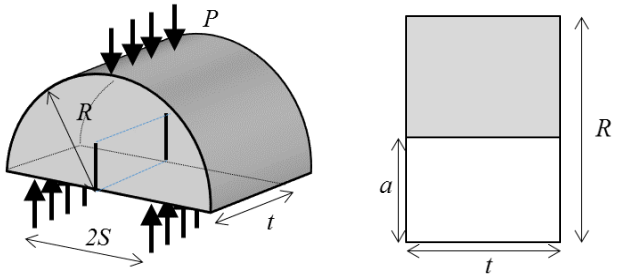

(a) STNSCB specimen

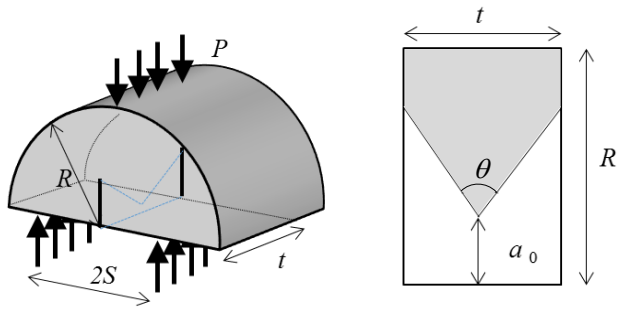

(b) CCNSCB specimen

Fig.1. Three points loading and geometry of artificial notch in cross section of specimen center; (a) STNSCB specimen, (b) CCNSCB specimen.

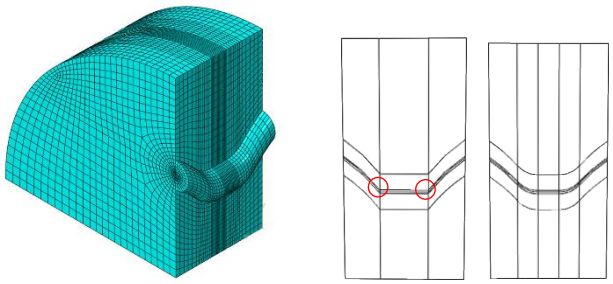

(a) (b) (c)

Fig.2 A finite element mesh and geometry of chevron notch: (a) 3D FEM model, (b) crack front with corners (Red circles), (c) modified crack front (Ayarollahi et al. 2016).

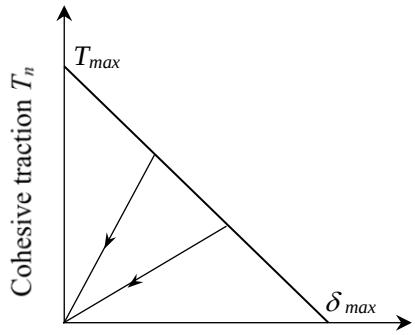

Fig.3 Typical linear traction-separation response.

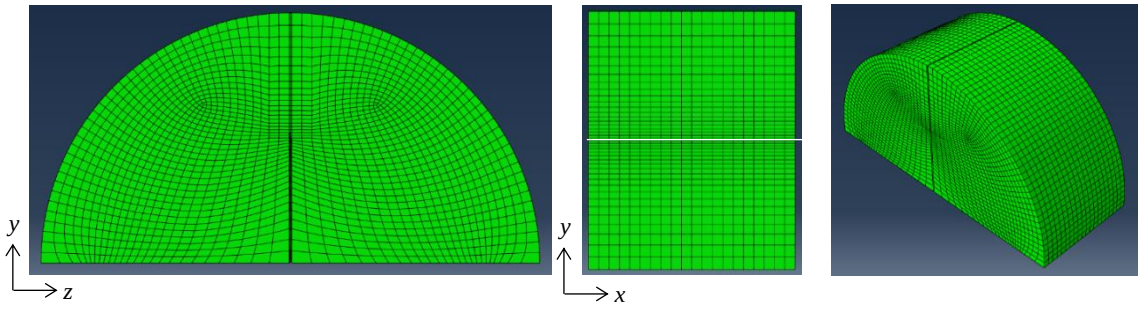

STNSCB specimen Straight

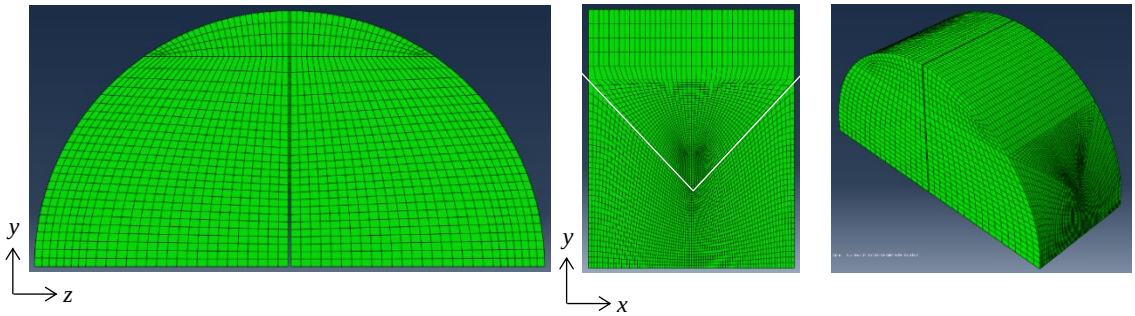

CCNSCB specimen (90) Angle 90 degrees

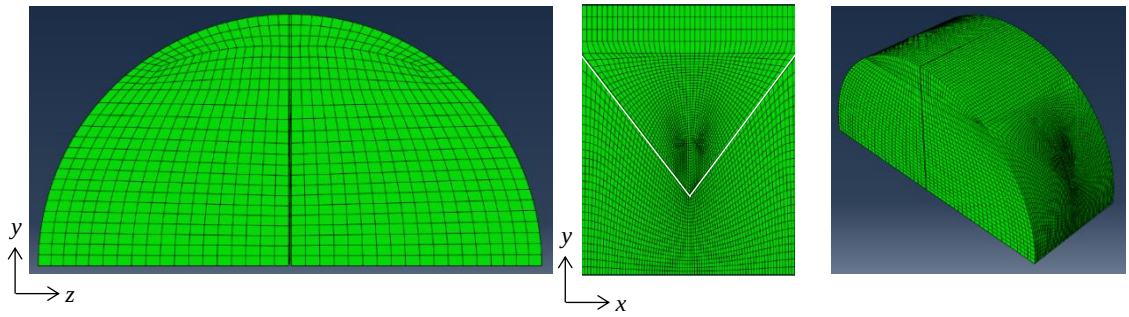

CCNSCB specimen (75) Angle 75 degrees

(a) on the *y*-*z* plane (b) in the *x*-*y* plane (c) 3D view

Fig.4 XFEM model: (a) cross section on the *y*-*z* plane, (b) perspective view of the crack front geometry in the *x*-*y* plane, (c) three dimensional view.

Table 1. Geometric and mechanical parameters.

Geometric parameter	value	
Radius of specimen R	37.5mm	
Thickness of specimen t	30.0mm	t/R = 0.8
Support distance 2s	60.0mm	s/R = 0.8
Initial crack length a_0	11.25, 18.75mm	a_0/R= 0.3, 0.5
Chevron angle θ	Straight, 90, 75 degrees	

Mechanical parameter	value
Young's modulus E	7.7GPa
Poisson's ratio ν	0.22

Table 2. Number of node and element of each model.

	STNSCB	CCNSCB(90)	CCNSCB(75)
Number of node	787469	125045	125045
Number of element	114209	111080	111080

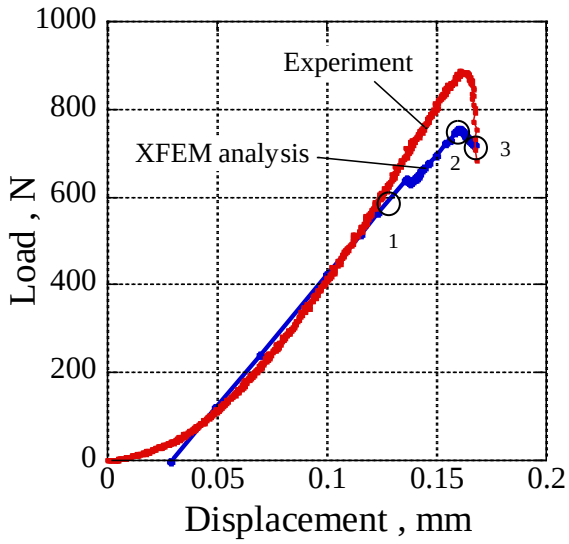

Fig.5 Comparison of load-displacement curve obtained from STNSCB test for sandstone with that by the XFEM analysis using model of STNSCB.

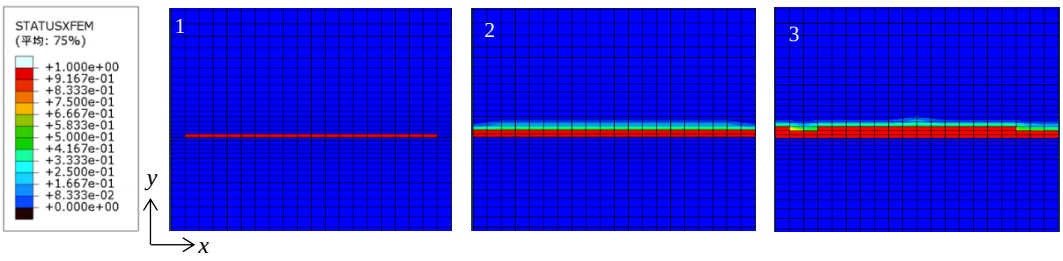

Fig.6 State of crack propagation at a moment of the numbers in Fig.5.

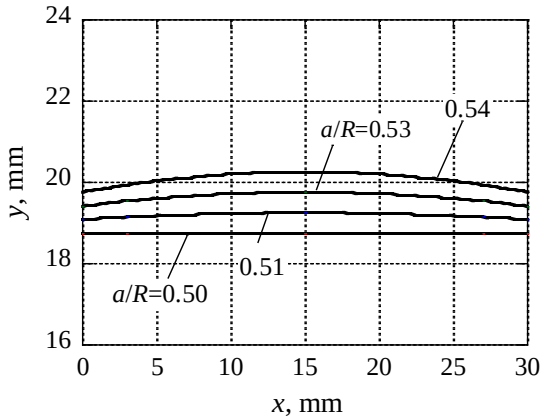

Fig.7 Cross sectional geometry of crack front during crack propagation of STNSCB test.

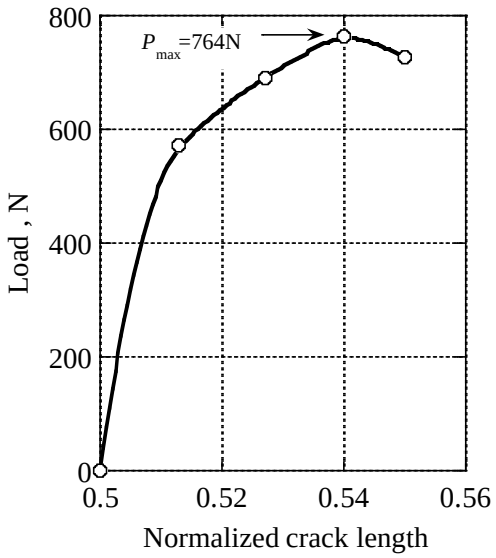

Fig.8 Load-crack length curve of STNSCB test.

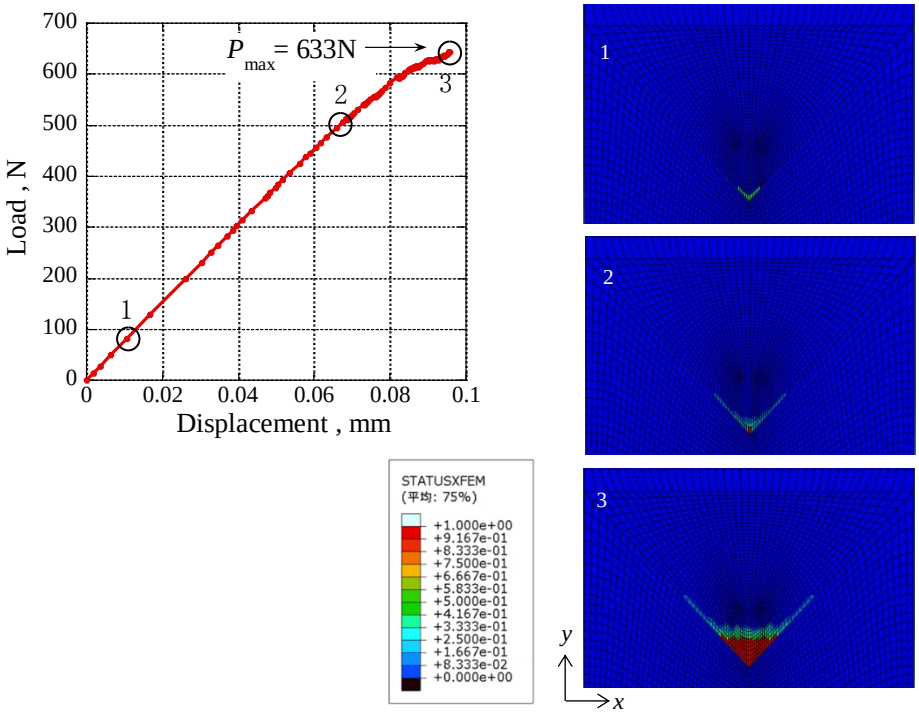

Fig.9 Load-displacement curve and states of crack propagation of CCNSCB specimen with a chevron angle of 90 degrees. Right figures represent the state of crack propagation at a moment of 1: P_{max}= 90kN, 2: 500kN and 3: 633kN.

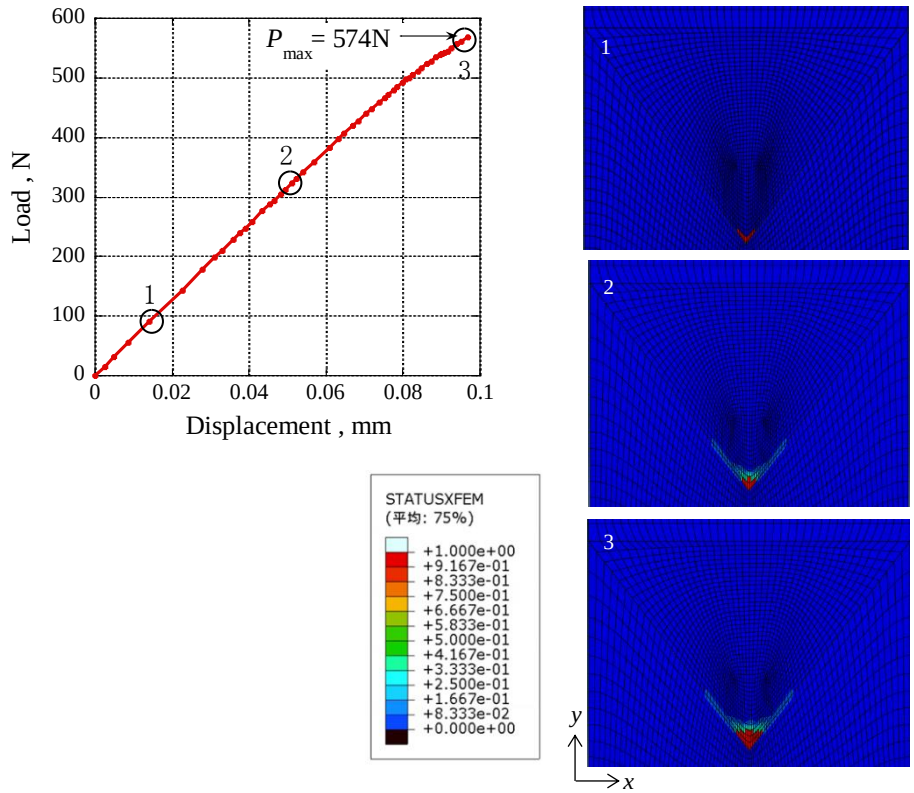

Fig.10 Load-displacement curve and states of crack propagation of CCNSCB specimen with a

chevron angle of 75 degrees. Right figures represent the state of crack propagation at a moment of 1: P_{max}= 90kN, 2: 310kN and 3: 574kN.

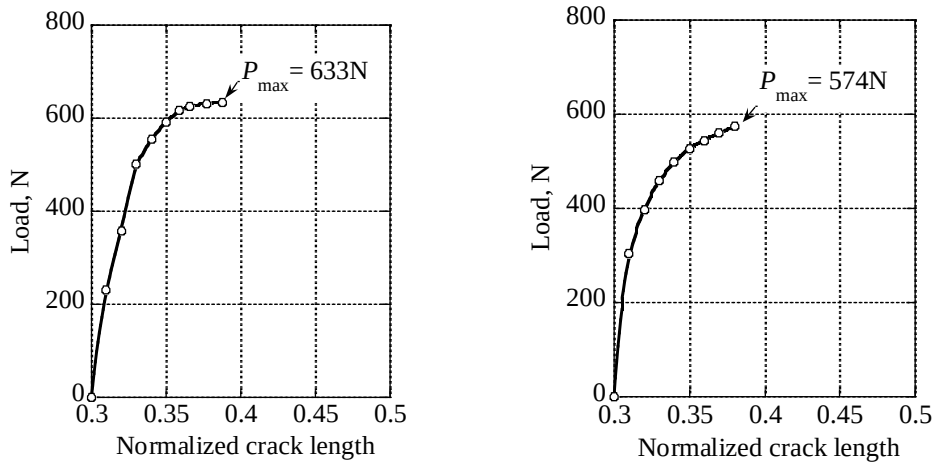

(a) chevron angle 90 degrees (b) chevron angle 75 degrees

Fug. 11 Relationship between load and normalized crack length a/R of CCNSCB models in the XFEM analysis.

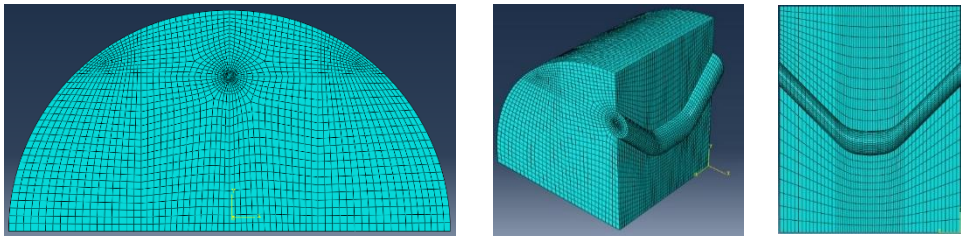

(a) cross section (b) bird eye view of half of the model (c) longitudinal section of the crack front geometry

Fig.12 An example of FEM model of CCNSCB specimen with a crack length of a/R=0.38 of chevron angle of 90 degrees.

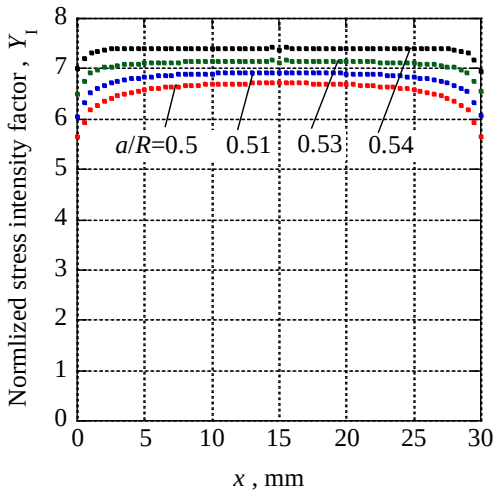

Fig.13 Distribution of normalized stress intensity factor along crack front shown in Fig.7 with increasing crack length in the STNSCB test.

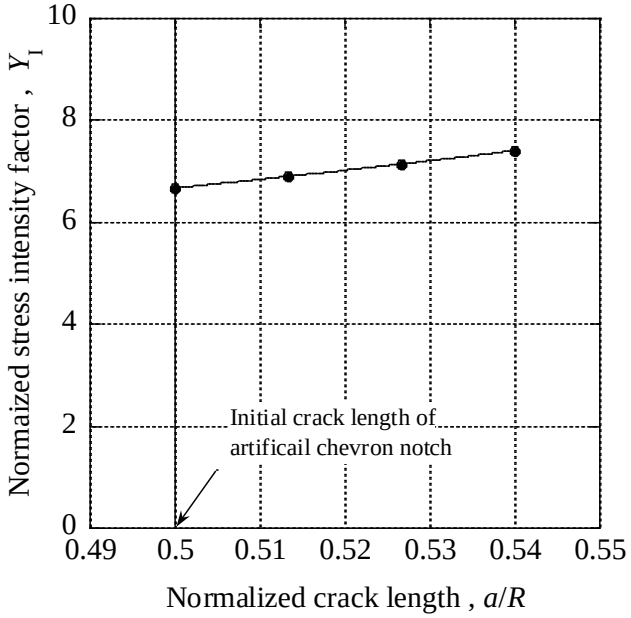

Fig.14 Relation between normalized stress intensity factor and normalized crack length in STNSCB test.

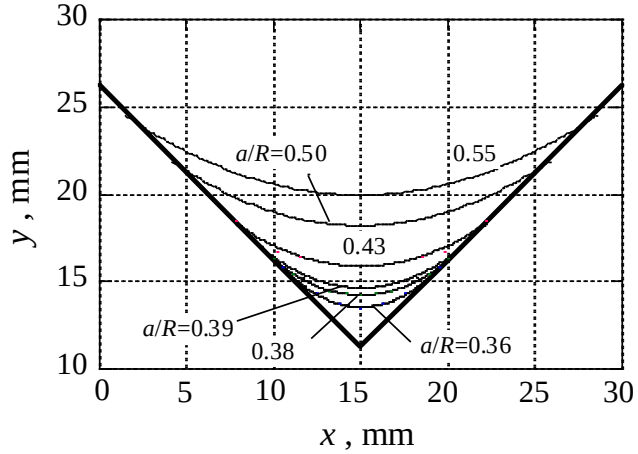

Fig.15 Cross-sectional geometry of the crack front for each crack length of the CCNSCB specimen with a chevron angle of 90 degrees obtained from the XFEM analysis.

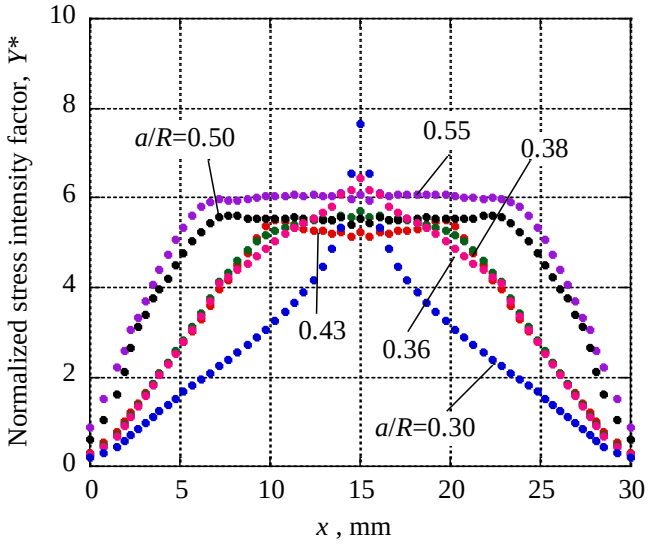

Fig. 16 Distributions of stress intensity factor in the range of 0.3 to 0.55.

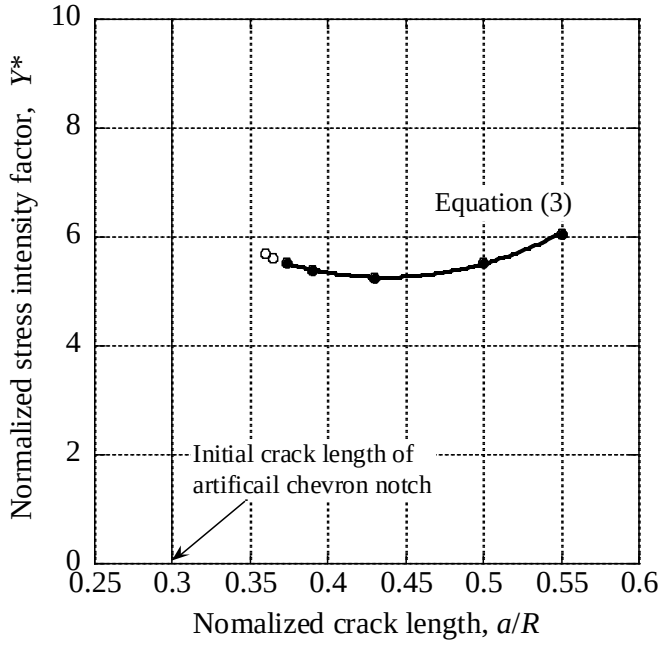

Fig.17 Relationship between normalized stress intensity factor with respect to a/R in the CCNSCB

specimen with a chevron angle of 90 degrees.

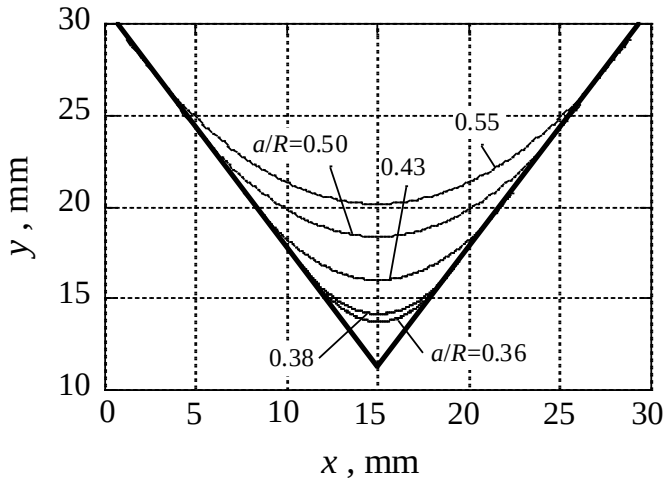

Fig.18 Cross-sectional geometry of the crack front for each crack length of the CCNSCB specimen with a chevron angle of 75 degrees obtained from the XFEM analysis.

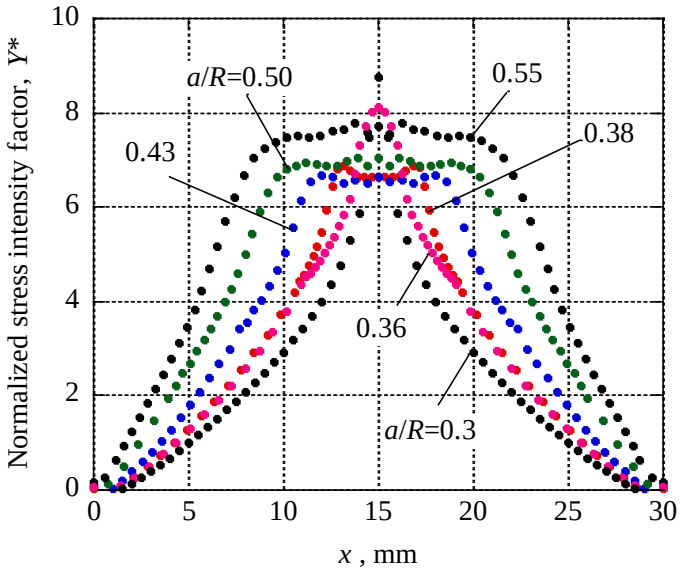

Fig. 19 Distributions of stress intensity factor in the range of 0.3 to 0.55.

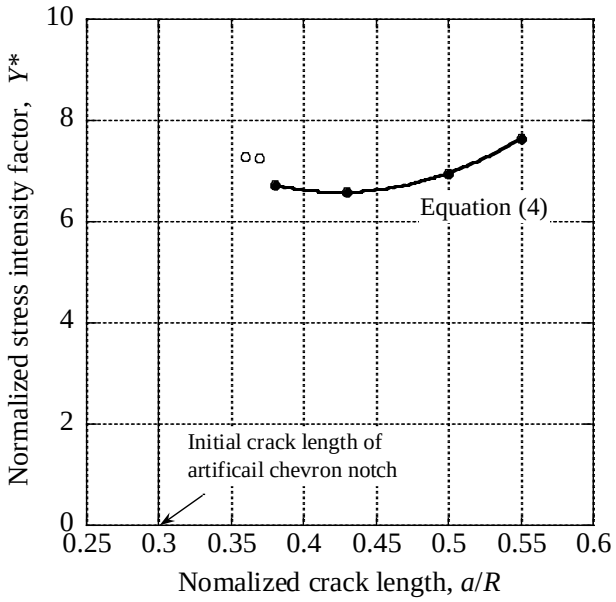

Fig.20 Relationship between normalized stress intensity factor with respect to a/R in the CCNSCB specimen with a chevron angle of 75 degrees.

Table 3 Material properties of Kimachi sandstone.

Material property	Values
Uniaxial compressive strength	59.3 MPa
Young's modulus	7.7 GPa
Poisson's ratio	0.22
Tensile strength	6.17 MPa
Elastic wave velocity	2.6–2.9 km/s

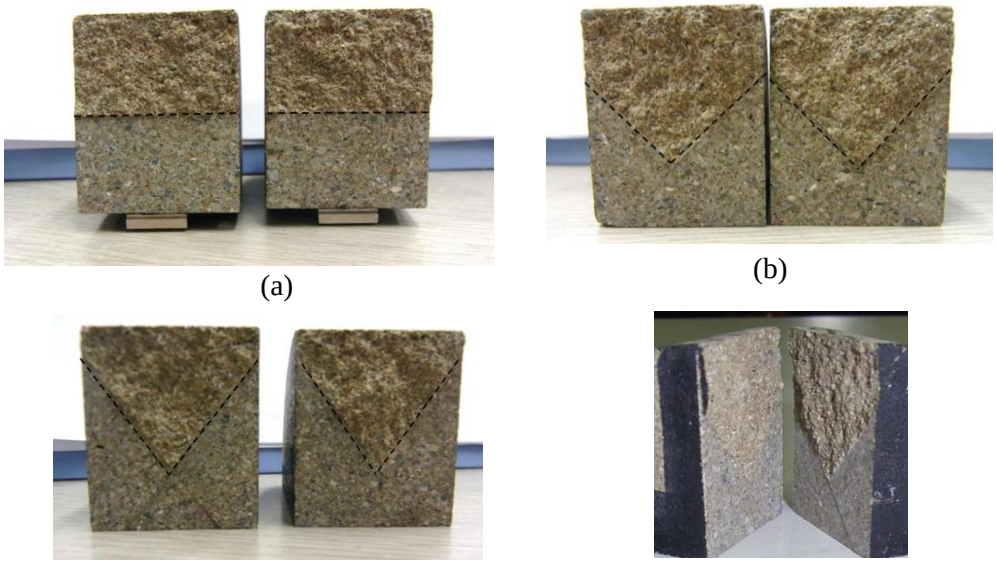

(a) (b) (c) (d)

Fig.21 Examples of fractured surface of STNSCB and CCNSCB specimens after test: (a) CSNSCB specimen, (b) CCNSCB specimen with a chevron angle of 90 degrees, (c) 75 degrees, (d) photo from an oblique direction.

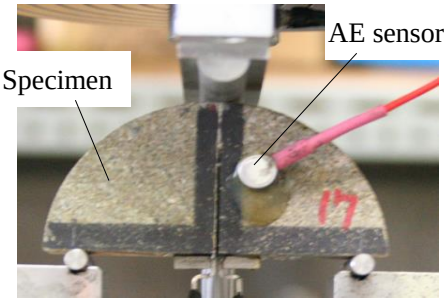

Fig.22 Loaded specimen attached an AE sensor.

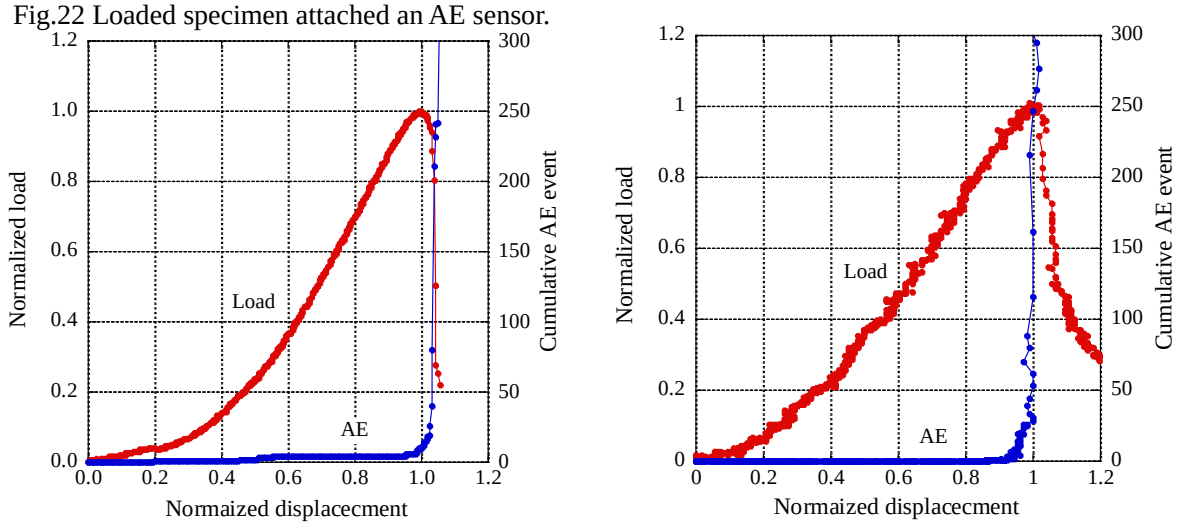

(a) (b)

Fig.23 Load and AE event rate – displacement curves: (a) STNSCB test (b) CCNSCB test with a chevron angle of 90 degrees during the test.

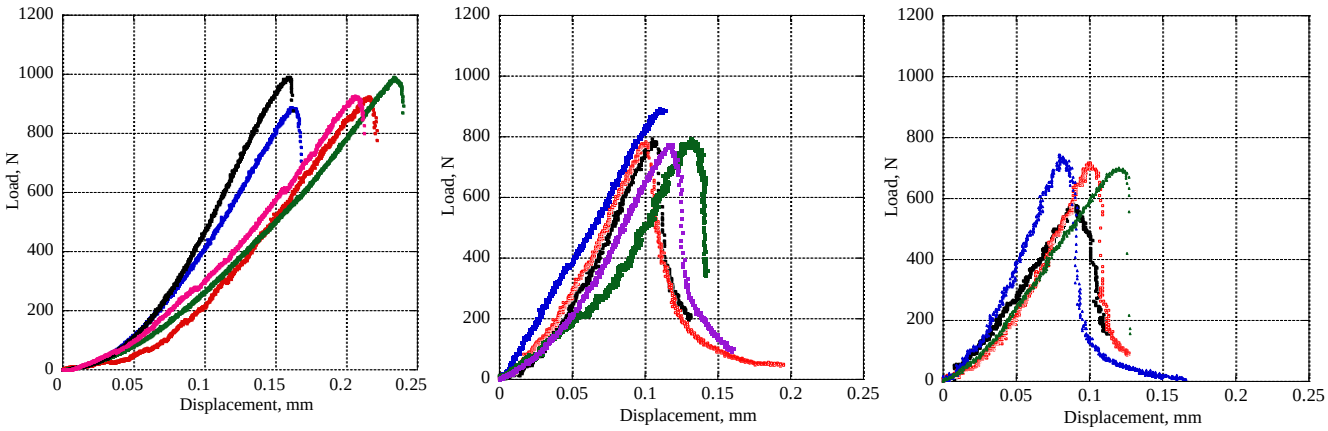

(a) (b) (c)

Fig.24 Load-displacements curves obtained SCB test: (a) STNSCB specimen, (b) CCNSCB specimen with a chevron angle of 90 degrees and (c) 75 degrees.

Table 4 Results of STNSCB test.

No.	Radius R, mm	Thickness t, mm	Crack length a_0, mm	a_0/R	$2S/R$	Y_I	Max. load P_{max}, kN	Fracture toughness K_{IC}, MN/m$^{3/2}$
1	37.5	30.4	19.8	0.53	0.8	7.09	0.93	0.72
2	37.5	30.4	19.8	0.53	0.8	7.09	0.92	0.71
3	37.5	30.9	19.7	0.53	0.8	7.04	0.89	0.67
4	37.5	30.9	19.6	0.52	0.8	7.00	0.99	0.74
5	37.5	31.5	19.7	0.53	0.8	7.04	0.98	0.73

Remarks: Y_I was calculated by the original formulation of ISRM (Kuruppu, Obara *et al*. 2014).

Table 5 Results of CCNSCB(90) test.

No.	Radius R, mm	Thickness t, mm	Crack length a_0, mm	a_0/R	$2S/R$	Y_I	Max. load P_{max}, kN	Fracture toughness K_{IC}, MN/m$^{3/2}$
1	36.4	30.6	10.7	0.29	0.8	5.26	0.77	0.69
2	36.3	31.6	10.0	0.28	0.8	5.26	0.79	0.69
3	36.6	31.2	11.1	0.30	0.8	5.26	0.89	0.78
4	36.2	30.9	10.1	0.28	0.8	5.26	0.78	0.70
5	37.1	30.0	11.1	0.30	0.8	5.26	0.79	0.72

Table 6 Results of CCNSCB(75) test.

No.	Radius R, mm	Thickness t, mm	Crack length a_0, mm	a_0/R	$2S/R$	Y_I	Max. load P_{max}, kN	Fracture toughness K_{IC}, MN/m$^{3/2}$
1	35.7	30.1	10.7	0.30	0.8	6.58	0.58	0.67
2	36.0	30.4	10.8	0.30	0.8	6.58	0.72	0.82
3	36.8	30.4	11.4	0.31	0.8	6.58	0.74	0.83
4	36.3	30.9	11.3	0.31	0.8	6.58	0.70	0.78

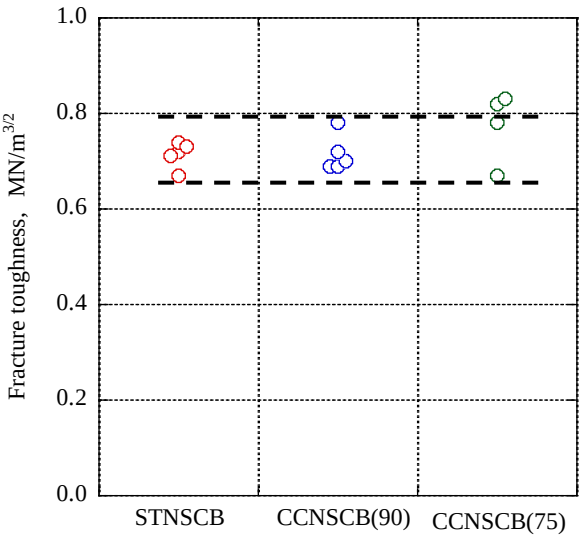

Fig 25 Fracture toughness of Kimachi sandstone estimated by the specimen with different artificial notch shape.